ISSN: 0067-2904

A Photometric and Spectroscopic Study of IC 2473, an Outer Pseudo-ring Galaxy (R'_1)

Zeinab F. Hussein*, Abdullah K. Ahmed
Department of Astronomy and Space, College of Science, University of Baghdad, Baghdad, Iraq

Received: 11/11/2024 Accepted: 22/5/2025 Published: 30/3/2026

Abstract

This work aims to study the outer Pseudo-ring galaxy IC 2473 by analyzing its spectroscopic and photometric data using griz filters from the Sloan Digital Sky Survey (SDSS). The ellipse task from the STSDAS library was applied within the IRAF environment to analyze the isophotes and extract the galaxy's structural and optical properties using surface photometric techniques. This analysis helped determine important parameters such as ellipticity, surface brightness, and position angle, enabling a precise characterization of the galaxy's structure.

A least-square fitting method was used to effectively study the morphological features. Spectroscopically, the emission line flux [OII] was analyzed to estimate the star formation rate (SFR), which was found to be approximately 0.124 $M_{\odot}$ yr^{-1}. The mass of the supermassive black hole (M_{BH}) was calculated using the M–σ relationship, and it was approximately 2.2×10^{7} $M_{\odot}$, with a Schwarzschild radius of 6.5×10^{7} km. In addition, the effective density of the black hole ($\rho_{\_BH}$) within the Schwarzschild radius was calculated and found to be approximately 3.75×10^{4} kg/m^{3}.

This study provides a comprehensive and integrated analysis of the structural, physical, and dynamical aspects of IC 2473, contributing to our understanding of the internal structure of pseudo-ring galaxies and their associated stellar activity.

Keywords: Pseudo-ring galaxy, SDSS, IC 2473, supermassive black hole.

دراسة ضوئية وطيفية للمجرة IC 2473، ذات الحلقة الزائفة الخارجية(R'_1)

زينب فاضل حسين* , عبد الله كامل احمد
قسم الفلك والفضاء, كلية العلوم, جامعة بغداد, بغداد, العراق

الخلاصة

يهدف هذا البحث إلى دراسة المجرة IC 2473 ذات الحلقة الكاذبة الخارجية و ذلك من خلال تحليل بياناتها الطيفية والضوئية بأستخدام مرشحات griz من Sloan Digital Sky Survey (SDSS). تم تطبيق مهمة القطع الناقص لمكتبة STSDAS داخل نظام IRAF, لتحليل الخطوط متساوية السطوع و استخلاص الخصائص البنيوية والضوئية للمجرة, أعتماداً على تقنيات القياس الضوئي السطحي. ساعد هذا التحليل في تحديد معايير مهمة مثل الاهليجية و السطوع السطحي وزاوية الموضع، مما يُتيح توصيفاً دقيقاً لبنية المجرة. أستُخدمت طريقة ملائمة اقل قيمة مربعة لدراسة السمات الشكلية للمجرة. تم استخدام تدفق خط

*Email: zeinab.hussein@sc.uobaghdad.edu.iq

الانبعاث [OII] لتقدير معدل تكوّن النجوم (SFR) طيفيًا، وكانت القيمة الناتجة حوالي $0.124\ M_{\odot}\ yr^{-1}$. حُسبت كتلة الثقب الأسود فائق الكتلة (M_{BH}) باستخدام علاقة M−σ، ووُجد أنها تُقدر بحوالي 2.2×10^{7} $M_{\odot}$، بنصف قطر شوارزشيلد (R_s) يبلغ 6.5×10^{7} كم. بالإضافة إلى ذلك، حُسبت الكثافة الفعالة للثقب الاسود(ρ_{BH}) ضمن نصف قطر شوارزشيلد، و وُجد أنها تبلغ حوالي 3.75×10^{4} كغم/م^3. تُقدم هذه الدراسة تحليلاً شاملاً و متكاملاً للجوانب البنيوية والفيزيائية والديناميكية للمجرة IC 2473, مما يُساهم في فهمنا للبنية الداخلية لمجرات الحلقة الزائفة و النشاط النجمي المرتبط بها.

1. Introduction

Rings are closed, elliptical, or circular structures composed of stars and gaseous formations inside a disk, which are late-type galaxies [1]. They are closely linked to the development of spiral structures, which may elucidate why numerous ones are pseudo-rings composed of tightly coiled spiral arms. Galaxies have three primary types of rings: nuclear, inner, and outer, designated according to their location inside the disc and their relation to the bar [2], [3].

The lens possesses a subtle brightness gradient from its center to the sharp periphery [4]. Lens analogs are available for every kind of ring [5]. Similar features are observed in the ring lens, which appear as low-contrast ring-like structures with a slight brightness enhancement near the edge [6].

According to the galaxy classifications from the RC3 catalog (de Vaucouleurs et al. 1991) with recessional velocities under 3000 km s^{-1} , Buta & Combes (1996) [1] stated that the frequency of inner and outer rings in disk galaxies is around 40−47% and approximately 10%, respectively.

Buta et al. (2015) conducted morphological classifications of the Spitzer Survey of Stellar Structure in Galaxies [3], encompassing galaxies within 40 Mpc. Comerón et al. (2014) identified a global fraction of 25 ± 1% for inner features (rings and ring lenses) and 16 ± 1% for outer features [7]. Although ring lenses are more prominent in early forms (S0), the distribution of inner and outer rings encompasses a wide array of morphological types, with a peak observed in Sa galaxies [5], [8].

Bars are among the most prominent dynamical structures in disk galaxies. They are believed to play a central role in redistributing angular momentum and driving gas inflow, which can lead to the formation of rings. In the local Universe, bars are observed in approximately two-thirds of disk galaxies [9]. Specifically, the bar fraction in Sb-Sc galaxies ranges between 40% and 45%. Infrared surveys, such as the Spritzer Survey of Stellar Structure in Galaxies (S4G), confirm that bars are even more frequent in late-type galaxies when observed in longer wavelengths, due to reduced dust obscuration and clearer tracing of the stellar mass distribution. The presence of a bar is often associated with resonance phenomena, which are closely linked to the development of nuclear, inner, and outer rings [10].

Strongly barred galaxies are expected to host larger or more extended rings compared to weakly barred or non-barred galaxies [11]. Grouchy et al. (2010) supported this prediction by analysing the ratio of tangential-to-radial force as, a proxy for bar strength. Their findings suggested a correlation between bar strength and ring size, although the study was limited by a relatively small sample (44 galaxies) [12].

Furthermore, Comerón et al. (2014) observed that when the galaxy classification shifts from SA (non-barred) to SB (very barred), the inner and outer rings increasingly exhibit elliptical shapes [7].

Since the foundational classification by de Vaucouleurs (1959a) and Sandage (1961), a major refinement in the categorization of ringed galaxies has involved the subtypes of outer rings and pseudo-rings in barred galaxies [13]. These morphological features bear a strong resemblance to the gaseous rings and pseudo-rings that formed near the outer Lindblad resonance (OLR) in Schwarz's test-particle simulations by Schwarz (1981; 1984), supporting the idea that such structures are dynamically induced by bar-driven resonances [11].

The photometric analysis conducted using the Image Reduction and Analysis Facility (IRAF) software package plays a pivotal role in this study. IRAF is a widely used software system for reducing and analysing astronomy data. In this study, we used the ellipse task from the STSDAS library to extract isophotal metrics such as ellipticity, position angle, and surface brightness profiles. This approach enabled a thorough analysis of the galaxy's morphological aspects, including its inner and outer structures. By using IRAF's powerful capabilities, we guaranteed exact photometric measurements, which are crucial for understanding the galaxy's physical features and confirming our results within the larger context of galaxy shape and development.

IC 2473, the barred spiral galaxy, is located in the Leo constellation. IC 2473 is more readily seen from the Northern Hemisphere since it is situated north of the celestial equator.

In accordance with the CVRHS classification, Buta (2017) [14] classified the barred galaxy IC 2473 as (R'_1)SB(r,bl)ab, corresponding to a type 1 outer pseudo-ring structure associated with the outer Lindblad resonance (OLR). HyperLEDA and NASA/IPACK Extragalactic Database (NED) also list this galaxy as UGC 05038; KUG 0924+306; CGCG 151-082; CGCG 152-001. Table 1 provides IC 2473's fundamental information.

Table 1: The IC 2473 Galaxy's Fundamental Information.

IC 2473	
Morphology	SB(r)bc *
CVRHS classification	(R'_1)SB(r,bl)ab ****
RA (deg)	141.847902 *
DEC (deg)	30.440814 *
Redshift	0.027 *
Semi major axis (kpc)	71.76 *
Inclination (deg)	48.6 **
Position Angle (deg)	92 **
Apparent magnitude in B-band (mag)	14.29 **
SDSS Name	SDSS J092723.49+302626.9***

*** NED, ** HyperLEDA, ***SDSS, ****Buta 2017 [14].**

Data Releases (DR7 and DR17) provided by the Sloan Digital Sky Survey (SDSS) include the observational spectroscopic data and photometric data in g, r, i, and z filters of the galaxy that make up the inner ring and outer pseudoring [15], [16]. The SDSS imaging data undergo a series of automated processing steps using the SDSS pipeline [17], [18]. As seen in Figure 1, the galaxy has an outer pseudoring of the R'_1 type, an inner ring, and a bar.

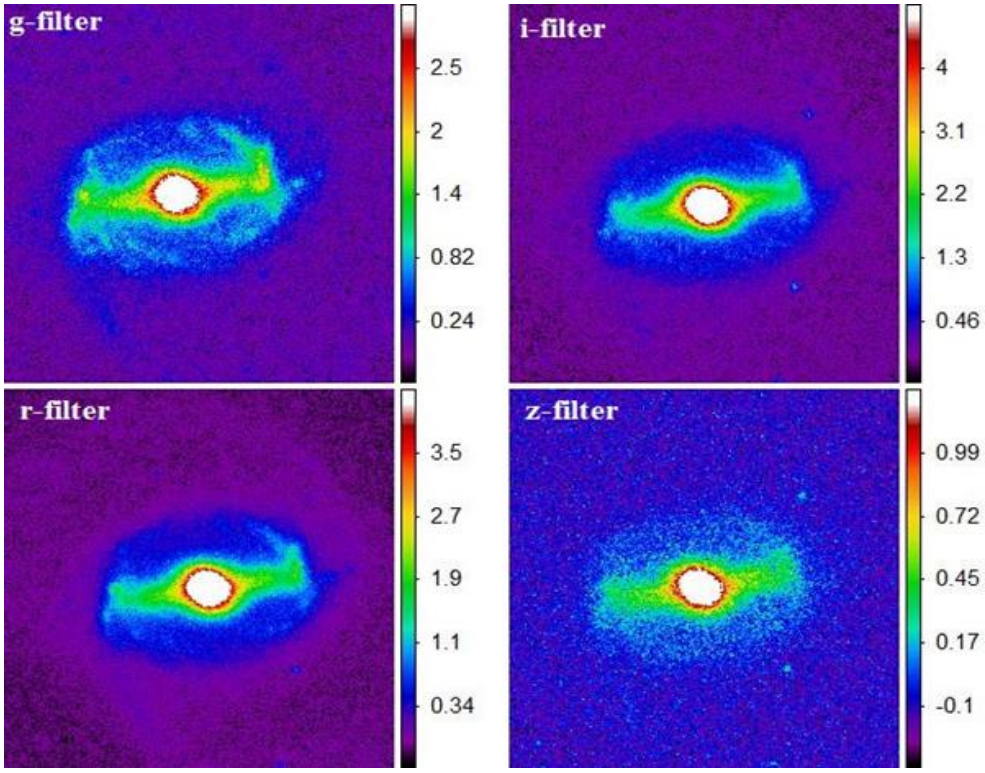

Figure 1: From left to right, fuzzy color photos of IC 2473 using griz-filters. East is left, and North is up.

1. Reduction of Data

The following procedures were used to reduce the observation data of the galaxy picture frames:

• Using IRAF's "imcopy" function, the target galaxy was chopped from the observed frames into new rectangular frames.

• Each galaxy frame's sky background intensity was deducted using IRAF's "imexam and imarith" routines.

• Each galaxy frame's pixels were translated to arcsec^2 units.

• By using IRAF's "imarith" function to divide each frame by its original exposure time, the flux was normalized to counts per second, standardizing the exposure duration to one second.

• Transform the intensity flux value (I) of each filter in the galaxy picture frames into magnitude units (m). Calibrate each galaxy picture frame for galactic and atmospheric extinction. Subsequently, apply Eq. (1) to multiply the flux data by the correction factors to convert them to the standard system [19].

$$\boldsymbol{m = 2.5\, log\, \left(I * 10^{(z_p + k_a + airmass)}\right)} \quad (1)$$

Where the atmospheric extinction is denoted by (k_a) and the zeropoint magnitude by (z_p). Table 2 provides zero-point magnitude (z_p), an atmospheric extinction (k_a), and an airmass for IC 2473 galaxy.

Table 2: The zero-point magnitude (z_p), an atmospheric extinction (k_a), and an airmass for IC 2473 galaxy [20].

Galaxy	filters	air mass	z_p	K_a
IC 2473	g	1.053003366	-24.566	0.136754
	r	1.047100662	-24.0571	0.0908142
	i	1.048539992	-23.6409	0.0368383
	z	1.051490492	-21.9969	0.0453443

2. Results and Discussion

2.1. IC 2473 Morphologies and Contour Maps

The isophotal contour maps of IC 2473, which is classified as $(R'_1)SB(r,bl)ab$, are displayed for the g, r, i, and z filters in Figure 2. These maps show the photometric structure of the galaxy, with a central region having an elliptical isophote corresponding to the bright bar and inner ring. As the contours extend outward, they outline the less luminous outer pseudo-ring (R'_1) formed by the spiral arms. The change in the shape of the isophotes across the filters reflects differences in stellar populations and dust extinction, with the (g) filter highlighting younger, bluer stars, while the (i) and (z) filters track older, redder stellar populations. These maps provide important insights into the photometric properties and morphological features of IC 2473. Table 3 lists the levels of surface brightness of IC 2473.

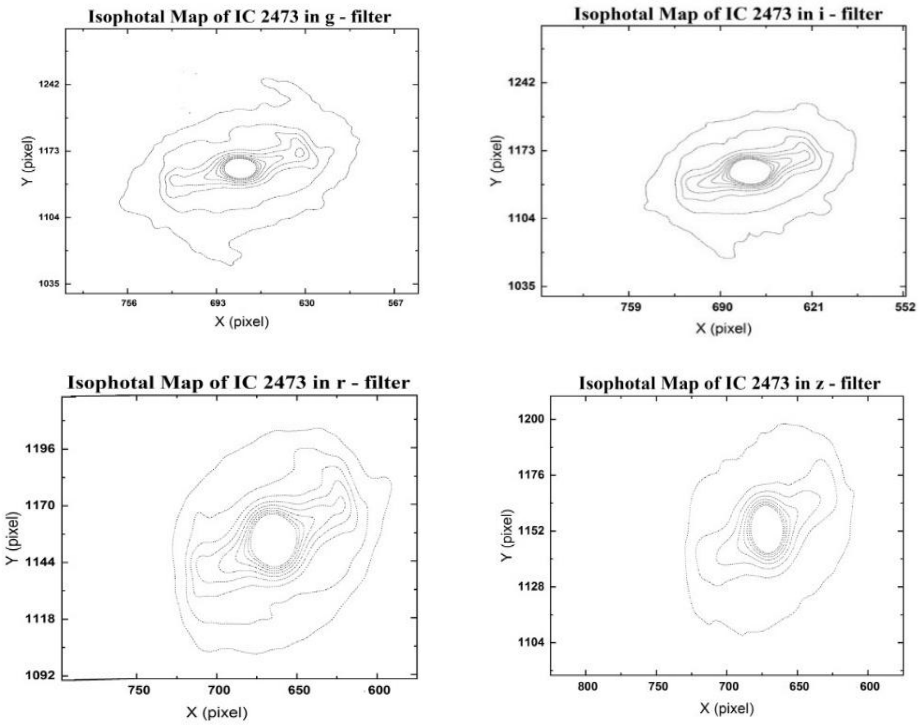

Figure 2: Isophotal Contour Maps of IC 2473 in griz-filter, North is up and East is left.

Table 3: The surface brightness levels of the griz outer isophotes of the IC 2473.

Galaxy	Filters	Surface brightness of Outer isophot (mag/arcsec ^{2})	Apparent magnitude of Outer isophot (mag)	Step
IC 2473	g	21.6579	23.66942	0.216
	r	20.71196	22.72349	0.55
	i	20.0857	22.09722	0.438
	z	19.9378	21.94933	0.105

2.2. Structural Parameters

The distributions of magnitude, Fourier coefficient (B4), position angle (PA), and ellipticity are presented in Figure 3, arranged in a clockwise direction starting from the top left quadrant. The overall distribution pattern of each parameter is nearly the same across all filters.

Figure 3, top left, shows the surface brightness curves of IC 2473 in the g, r, i, and z filters. The magnitude values show that the galaxy is brightest in the center and gradually becomes dimmer toward the periphery. As the radius increases, the magnitude values rise steadily up to about 4.1546 arcsec, which may indicate the presence of the inner ring (r)

surrounding the bar. The inner rings are typically moderately bright and less luminous than the bar. At about 6.4851 arcsec, a more pronounced increase in magnitude is observed, indicating a more rapid decrease in brightness, and this may represent the location of the outer pseudoring (R'_1) formed by the spiral arms. The high magnitude values in the outer regions, up to ~24.4, confirm that this ring is less dense and less luminous than the inner regions of the galaxy.

The B4 parameter in the core region of a galaxy is nearly elliptical, as seen in Figure 3, top right. In the central regions (1–4 arcsec), values close to zero show an elliptical-shaped isophot, consistent with a central lens (bl) and a regular bulge. In the intermediate range (about 2–6 arcsec), the galactic bar (SB) is likely to extend. The observed high B4 values in the outer regions (6.9–10.4 arcsec) reflect the influence of the outer pseudo-ring (R'_1) or spiral arms.

The position angle (PA) in the center area of Figure 3, bottom left, begins at 156.8° and progressively drops to around 128.74°. A bar-dominated core area is consistent with the rather constant trend shown by this gradual change in PA. The inside of bars often maintains a steady trend, which can only slightly alter PA. The PA values start to vary at (2.5 arcsec). An external oscillation (class "R'_1") that might lead to distortions or deviations in the galaxy's direction may be the origin of these fluctuations. These variations in the PA might be brought on by the oscillations' frequent lack of absolute symmetry. The outer disk, including the outer pseudoring, has a rather consistent orientation at higher diameters, as seen by the PA stabilizing at around 163.7º after (6) arcsec.

The ellipticity of the IC 2473 galaxy at intermediate luminosities was recorded by multiband photometric observations using the SDSS griz filter. These data help identify features such as bars, rings, and spiral arms. The central region has an ellipticity close to zero, indicating a circular shape. The intermediate region gradually increases in ellipticity, corresponding to the inner ring. The outer region has a significant increase in ellipticity, reaching a peak of about 0.6 at $r\sim10$ arc sec before stabilizing. This peak ellipticity is associated with an outer pseudo-ring (R'_1) consisting of spiral arms, indicating the influence of these arms and the disk structure at larger radii, as seen in Figure 3, bottom right.

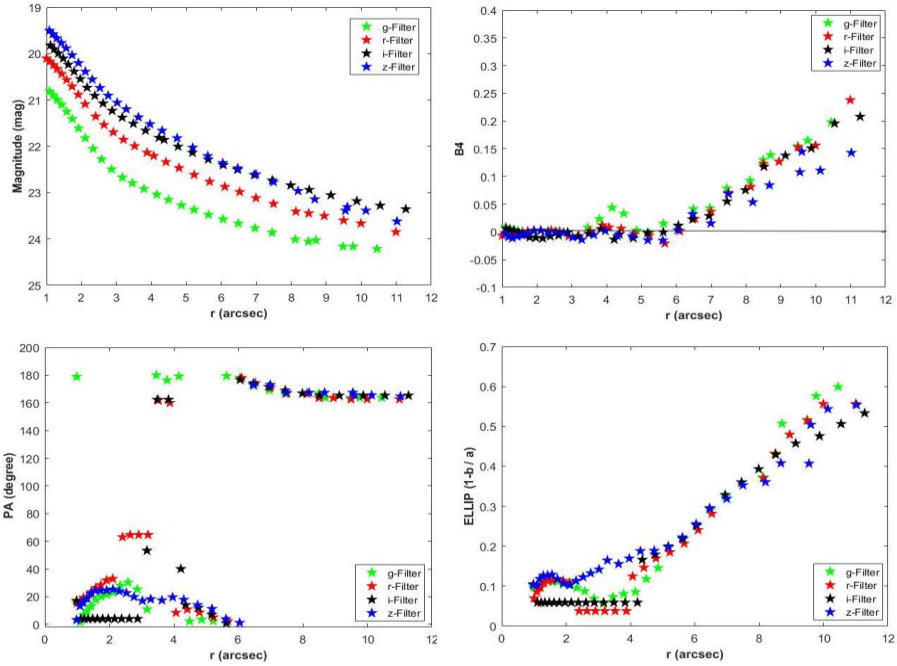

Figure 3: The magnitude (top left), Fourier coefficient (B_4) (top right), position angle (PA) (lower left), and ellipticity (lower right) as a function of the semi-major axis of the IC 2473 galaxy.

2.3. Surface Brightness Profiles Decomposition

De Vaucouleur's law $r^{1/4}$, which simulates the circular reduction in surface brightness with radius, is often used to characterize a galaxy's center bulge. Eq. (2) may be used to express this law [21]:

$$\boldsymbol{\mu_{bulge}(r) = \mu_e + 8.3268 \left[\left(\frac{r}{r_e}\right)^{1/4} - 1\right]} \quad (2)$$

Eq. (3) shows that the disk's brightness profile is exponential [21].

$$\boldsymbol{\mu_{disk}(r) \ = \mu_0 + 1.09 \left(\frac{r}{r_0}\right)} \quad (3)$$

At effective radius r_e, when half of the light is radiated inside r_e, the surface brightness is denoted by μ_e. The symbols μe and r_0 stand for the center surface brightness and disk scale length, respectively. It should be mentioned that μ_0 is not directly measured because it only represents the brightness of the disk component and not the galaxy's center surface.

The relationship between the galaxy radius (r) in the griz filters and the surface brightness fit of the bulge and disk structure of the IC 2473 is seen in Figure 4. Table 4 presents the findings as well. The IC 2473's surface brightness profiles indicate that these galaxies' outer disks were type I Freeman [22].

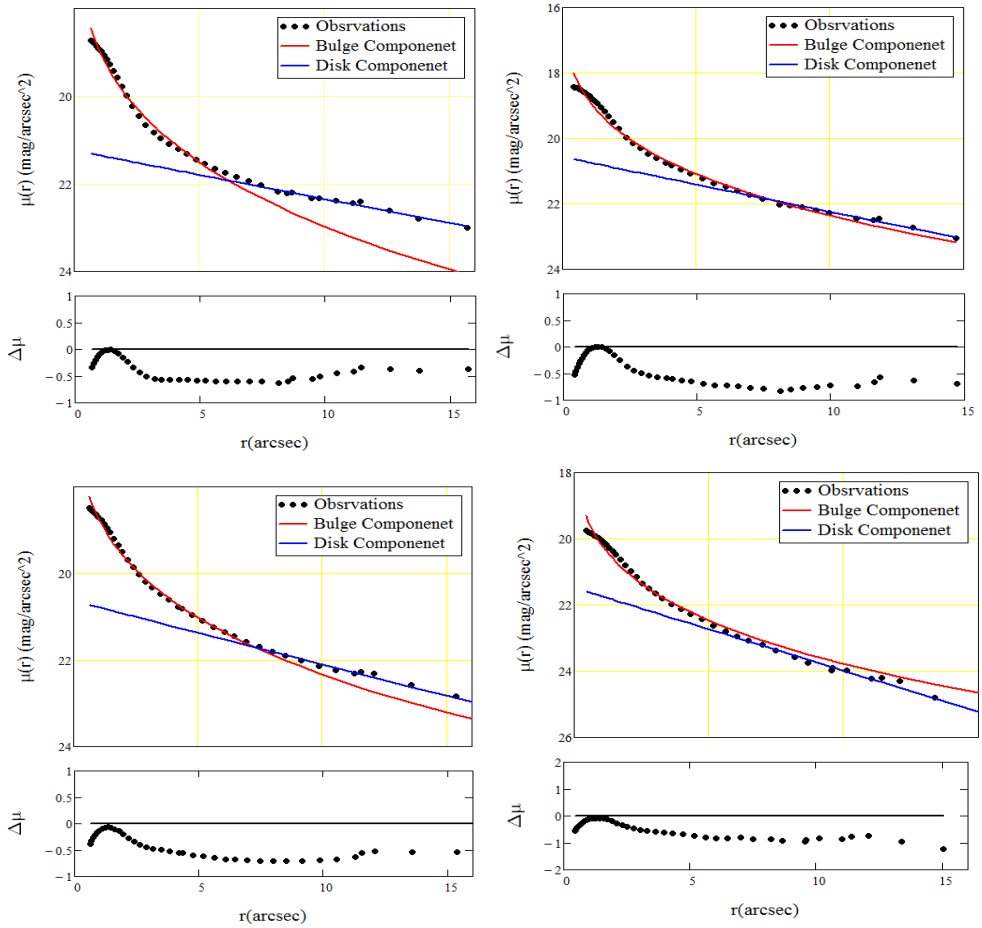

Figure 4: Decomposition of griz-band surface brightness profiles between the observed data for the IC 2473 galaxy and the (Bulge+Disk) model. From top left to right, griz-filters.

Table 4: IC 2473's Decomposition Parameters.

		Bulge				Disk				
	Filter	Range (arcsec)	μ_e (mag/arcsec^2)	r_e (arcsec)	Standard error	μ_o (mag/arcsec^2)	r_o (arcsec)	Standard error	LB_T (mag)	B/D
IC 2473	g	0.746-6.048	22.083	6.653	0.046	21.245	9.846	0.017	14.58	0.4
	r	0.472-5.667	22.674	11.664	0.064	20.57	6.496	0.026	13.951	0.881
	i	0.686-6.054	22.412	10.363	0.035	20.637	7.413	0.021	13.946	0.723
	z	0.492-6.039	23.832	10.262	0.064	21.481	4.341	0.04	15.387	1.217

2.4. Color index

The color index is an important property that provides information on the populations and age of stars within galaxy profiles. In this study, the color profiles g-r, r-i, and i-z, are shown along the semi-major axis in Figure 5.

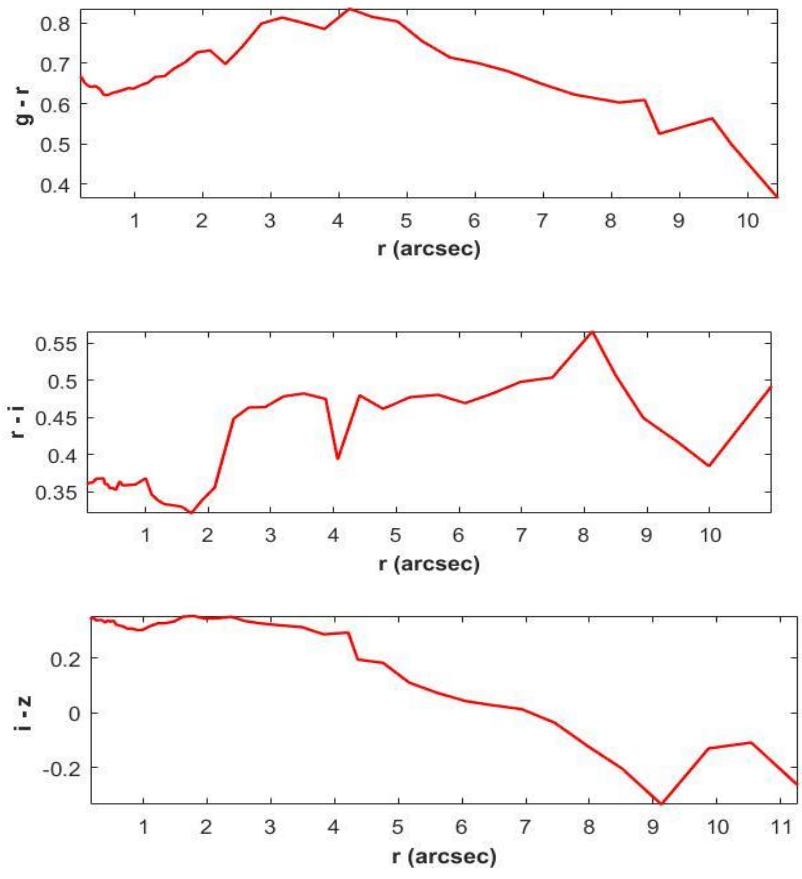

Figure 5: g-r, r-i, and i-z color profiles of IC2473.

The (g-r) values are quite constant, beginning at around 0.6670 and then slightly decreasing to about (0.6335) before increasing once again. At three to four arcseconds, the g-

r color peaks at around 0.8349. The (g-r) values gradually drop beyond about 7 arcseconds, reaching 0.3652 at the farthest radius (~10 arcsec).

The r-i color distribution in the inner regions of the galaxy is flat, with values of about 0.33-0.37. The peak at 8 arcseconds reaches 0.55, indicating a mixture of middle-aged and old stars. The number of stars in the outer regions is reduced, probably due to a younger population of stars and a lower dust content. The (i-z) values gradually decrease from 0.35 (near the center of the galaxy) to negative values ~ (-0.33) towards the outer regions. This indicates changes in the star population along the semi-major axis, which likely correspond to different structural components of the galaxy.

2.5. Star Formation Rate Calculation of IC 2473

One of the most significant processes in a galaxy's creation is star formation. Due to their dependence on the brightness of ionizing photons, the luminosities of [OII] were utilized to determine the star formation rate (SFR) [23].

$$\mathbf{SFR}_{[OII]}\ (\mathbf{M}_{\odot}\ \mathbf{yr}^{-1}) = \frac{\mathbf{L}_{[O\ II]}\ erg.\ s^{-1}}{\mathbf{2.97\times10^{33}\ W}} \quad (4)$$

To calculate the luminosities of [OII] [24]:

$$\boldsymbol{L}_{[O\ II]} = \mathbf{4\pi \times D_L^2 \times S} \quad (5)$$

Where S is the flux density for each [OII] line in units (erg. cm^{-2}. s^{-1}) and D_L is the luminosity distance in units (cm). By integrating the redshift with the cosmological parameters H_0 =70 km s^{-1}Mpc^{-1}, Ω_m = 0.3 (omega matter), and Ω_{vac} = 0.714 (omega vacuum), the luminosity distance (D_L) of the galaxy IC 2473 has been calculated [25]. The star formation rate (SFR) of the IC 2473 galaxy may readily be estimated using Eqs. (4, 5), with the findings presented in Table 5.

Table 5: The luminosity distance, flux density, luminosities of [OII], and the Star formation rate calculation of IC 2473

Name of galaxy	D_L (Mpc)	D_L (cm)	S * (erg. cm^{-2}. s^{-1})	$L_{[OII]}$ (erg.s^{-1})	$L_{[OII]}$ (W)	$SFR_{[OII]}$ ($M_{\odot}$ yr^{-1})
IC 2473	117.7	3.63×10^{26}	2.23×10^{-15}	3.69×10^{39}	3.69×10^{32}	0.124

***SDSS (DR 16)**

The emission lines of OII, OIII, NII, Hβ, Hα, and SII that were discernible in the IC 2473 galaxy's spectrum are displayed in Figure 5.

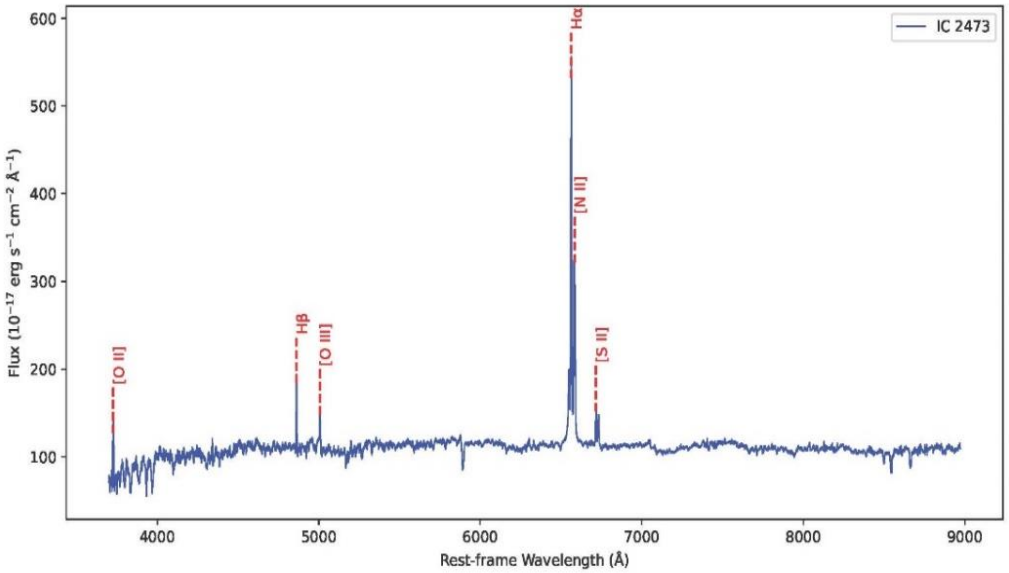

Figure 6 : Spectra of galaxy IC 2473.

2.6. Super Massive Black Hole's Mass Calculation in IC 2473

Several techniques are often used to determine the mass of a supermassive black hole (SMBH) in a galaxy like IC 2473. The most widely used techniques, however, need galactic characteristics like star velocity dispersion and observational data. The star velocity dispersion (σ) in the galactic bulge and the mass of the supermassive black hole (M_{BH}) are related by the M-σ relation. When the stellar velocity dispersion is known, this empirical relation is often used [26]:

$$M_{\mathrm{BH}} \approx 10^{8.13} \left(\frac{\sigma}{200 \frac{\mathrm{km}}{\mathrm{s}}} \right)^{4.24} \mathrm{M}_{\odot} \tag{8}$$

The following formula may be used to determine the supermassive black hole's Schwarzschild radius (R_s) at IC 2473 [27]:

$$R_s = \frac{2\,G\,M_{BH}}{C^2} \tag{9}$$

Where G represents the gravitational constant and c denotes the speed of light.

The following relation may be used to determine the escape velocity (v_{es}) close to the supermassive black hole in IC 2473 at the Schwarzschild radius (R_s) [28]:

$$v_{\mathrm{es}} = \sqrt{\frac{2\,G\,M_{\mathrm{BH}}}{R_s}} \tag{10}$$

Substituting Eq. (9) for the Schwarzschild radius into Eq. (10) for the escape velocity, we get Eq. (11).

$$v_{es} = \sqrt{c^2} = c \tag{11}$$

So, Eq. (11) shows that the escape velocity (v_{es}) at the Schwarzschild radius (R_s) is equal to the speed of light (c), which defines the event horizon of the black hole. Within this boundary, no object or radiation can escape as described by general relativity.

To calculate the density of the supermassive black hole (ρ_{BH}) in IC 2473, one can use a sphere density formula, which depends on the mass and volume of the black hole. The volume is approximated using the Schwarzschild radius as the radius of the black hole [27].

$$\rho_{BH} = \frac{3\,M_{\mathrm{BH}}}{4\,\pi\,.R_S^3} \tag{12}$$

Table 6: Dispersion of stellar velocity, mass, Schwarzschild radius, and density of the supermassive black hole in IC 2473

σ (km/s)*	M_{BH}	R_s (km)	ρ (kg/m^3)
130.69	2.2 ×10^7 M$_\odot$	6.5×10^7	3.75×10^4

***SDSS (DR 16)**

3. Conclusions

The most important conclusions of this study are as follows:

- IC 2473's brightness pattern corresponds with its structural features.
- IC 2473's position angle (PA) examination shows clear areas of stability and variation in the galaxy's structure.
- Our study indicates that IC 2473's outer disks have a type I Freeman brightness profile.

- The study of IC 2473 has yielded essential insights into several significant astrophysical properties. The star formation rate, ascertained from the [OII] emission line, offers an approximation of the galaxy's present star creation activity. Furthermore, the mass of the supermassive black hole (M_{BH}) is estimated to be roughly 2.2×10^7 $M_\odot$, resulting in calculations of the Schwarzschild radius (R_s) of the black hole. These factors provide a more profound insight into the black hole's impact on the galaxy's dynamics. Additionally, the density of the supermassive black hole (ρ_{BH}) has been ascertained, offering insights into the black hole's exceptional compactness. Collectively, these computations enhance our comprehension of the dynamics of the center area and the overarching gravitational and evolutionary mechanisms inside IC 2473.
- The escape velocity of the black hole at IC 2473 is equal to the speed of light, demonstrating that nothing, including light, can escape from inside the black hole's Schwarzschild radius.

Acknowledgment

We express our gratitude to the Sloan Digital Sky Survey (SDSS) for supplying the observational data used in this investigation. This study used the NASA/IPAC Extragalactic Database (NED), managed by the Jet Propulsion Laboratory at the California Institute of Technology, under contract with the National Aeronautics and Space Administration (NASA). Furthermore, we used NASA's Astrophysics Data System Bibliographic Services. We recognize the use of the HyperLeda database (http://leda.univ-lyon1.fr).

References

[1] R. J. Buta and F. Combes, "Galactic rings," 1996.

[2] S. M. Qasim and H. S. Mahdi, "Investigating the Color Distribution of Young and Old Galaxies Using Observations from SDSS," *Iraqi Journal of Science,* vol. 65, no. 4, pp. 2344-2356, 2024.

[3] R. J. Buta, K. Sheth, E. Athanassoula, A. Bosma, J. H. Knapen, E. Laurikainen, H. Salo, D. Elmegreen, L. C. Ho, and D. Zaritsky, "A classical morphological analysis of galaxies in the Spitzer survey of stellar structure in galaxies (S4G)," *The Astrophysical Journal Supplement Series,* vol. 217, no. 2, p. 32, 2015.

[4] J. Kormendy, "A morphological survey of bar, lens, and ring components in galaxies Secular evolution in galaxy structure," *Astrophysical Journal, Part 1,* vol. 227, pp. 714-728, 1979.

[5] E. Laurikainen, H. Salo, R. Buta, and J. Knapen, "Near-infrared atlas of S0-Sa galaxies (NIRS0S)," *Monthly Notices of the Royal Astronomical Society,* vol. 418, no. 3, pp. 1452-1490, 2011.

[6] A. H. Abdullah and P. Kroupa, "The Dichotomy of the Mass-radius Relation and the Number of Globular Clusters," *Astronomy letters,* vol. 47, no. 3, pp. 170-174, 2021.

[7] S. Comerón, H. Salo, E. Laurikainen, J. H. Knapen, R. J. Buta, M. Herrera-Endoqui, J. Laine, B. W. Holwerda, K. Sheth, and M. Regan, "ARRAKIS: atlas of resonance rings as known in the S4G," *Astronomy & Astrophysics,* vol. 562, p. A121, 2014.

[8] L. Y. A.-S. Mashhadani and A. H. Abdullah, "A Cosmological View for the Time-Variation of the Fundamental Constants of Nature," *NeuroQuantology,* vol. 18, no. 12, pp. 18-30, 2020.

[9] P. B. Eskridge, J. A. Frogel, R. W. Pogge, A. C. Quillen, A. A. Berlind, R. L. Davies, D. DePoy, K. M. Gilbert, M. L. Houdashelt, and L. E. Kuchinski, "Near-Infrared and Optical Morphology of SpiralGalaxies," *The Astrophysical Journal Supplement Series,* vol. 143, no. 1, p. 73, 2002.

[10] K. Sheth, M. Regan, J. L. Hinz, A. G. De Paz, K. Menéndez-Delmestre, J.-C. Muñoz-Mateos, M. Seibert, T. Kim, E. Laurikainen, and H. Salo, "The Spitzer Survey of Stellar Structure in Galaxies ()," *Publications of the Astronomical Society of the Pacific,* vol. 122, no. 898, p. 1397, 2010.

[11] M. Schwarz, "How bar strength and pattern speed affect galactic spiral structure," *Monthly Notices of the Royal Astronomical Society,* vol. 209, no. 1, pp. 93-109, 1984.

[12] R. D. Grouchy, R. Buta, H. Salo, and E. Laurikainen, "Ring Star Formation Rates in Barred and Nonbarred Galaxies," *The Astronomical Journal,* vol. 139, no. 6, p. 2465, 2010.

[13] E. Athanassoula, M. Romero-Gómez, A. Bosma, and J. Masdemont, "Rings and spirals in barred galaxies–II. Ring and spiral morphology," *Monthly Notices of the Royal Astronomical Society,* vol. 400, no. 4, pp. 1706-1720, 2009.

[14] R. J. Buta, "Galactic rings revisited. II. Dark gaps and the locations of resonances in early-to-intermediate-type disc galaxies," *Monthly Notices of the Royal Astronomical Society,* vol. 470, no. 4, pp. 3819-3849, 2017.

[15] K. Accetta, C. Aerts, V. S. Aguirre, R. Ahumada, N. Ajgaonkar, N. F. Ak, S. Alam, C. A. Prieto, A. Almeida, and F. Anders, "The seventeenth data release of the Sloan Digital Sky Surveys: Complete release of MaNGA, MaStar, and APOGEE-2 data," *The Astrophysical Journal Supplement Series,* vol. 259, no. 2, p. 35, 2022.

[16] A. Eckart, M. Horrobin, S. Britzen, M. Zamaninasab, K. Mužić, N. Sabha, B. Shahzamanian, S. Yazici, L. Moser, and M. García-Marin, "The infrared K-band identification of the DSO/G2 source from VLT and Keck data," *Proceedings of the International Astronomical Union,* vol. 9, no. S303, pp. 269-273, 2013.

[17] H. R. Al-baqir and A. K. Ahmed, "Explaining the photometric and spectroscopic properties of The Sip-39 galaxy pair," *Baghdad Science Journal,* vol. 21, no. 4, pp. 1403-1403, 2024.

[18] Y. Rashed, J. Zuther, A. Eckart, G. Busch, M. Valencia-S, M. Vitale, S. Britzen, and T. Muxlow, "High-resolution observations of SDSS J080800. 99+ 483807.7 in the optical and radio domains-A possible example of jet-triggered star formation," *Astronomy & Astrophysics,* vol. 558, p. A5, 2013.

[19] I. A. M. Ali, H. S. Mahdi, Z. Z. Abidin, and D. A. A. Lee, " Probing the Rotation Curve of NGC 4501 Galaxy using Two Different Models," *Malaysian Journal of Science,* vol. 44, no. 2, pp. 63- 68, 2025.

[20] A. Almeida, S. F. Anderson, M. Argudo-Fernández, C. Badenes, K. Barger, J. K. Barrera-Ballesteros, C. F. Bender, E. Benitez, F. Besser, and J. C. Bird, "The eighteenth data release of the sloan digital sky surveys: Targeting and first spectra from sdss-v," *The Astrophysical Journal Supplement Series,* vol. 267, no. 2, p. 44, 2023.

[21] H. B. Ann and H. W. Park, "Luminosity Profiles of Prominent Stellar Halos," *arXiv preprint arXiv:1807.04922,* 2018.

[22] K. C. Freeman, "On the disks of spiral and S0 galaxies," *Astrophysical Journal,* vol. 160, p. 811, 1970.

[23] S. H. Kareem and Y. E. Rashed, "Studying the Correlation between Supermassive Black Holes and Star Formation Rate for Samples of Seyfert Galaxies (Type 1 and 2)," *Iraqi Journal of Physics,* vol. 19, no. 48, pp. 52-65, 2021.

[24] M. Al Najm, Y. Rashed, and H. AL-Dahlaki, "Comparison of physical characteristics of mass and luminosity function of disk systems in barred and unbarred spiral galaxies," *Baghdad Science Journal,* vol. 21, no. 10, pp. 3277-3277, 2024.

[25] A. H. Abdullah, P. Kroupa, P. Lieberz, and R.A. González-Lópezlira, "On the primordial specific frequency of globular clusters in dwarf and giant elliptical galaxies," *Astrophysics and Space Science,* Vol. 364, No. 5, p. 86, 2019.

[26] M. N. Al Najm, A. H. Abdullah, and Y. E. Rashed, "Estimating the evolution and the content fractions of baryonic gas for luminous infrared galaxies," *Monthly Notices of the Royal Astronomical Society,* Vol. 537, No. 2, pp: 1597–1607, 2025.

[27] M. H. Al-kubaisy, "Using of the Correction Schwarzschild radius Equation and Its Application of the Black Holes," *Ibn AL-Haitham Journal For Pure and Applied Science,* vol. 27, no. 2, pp. 121-127, 2017.

[28] P. Schneider, *Extragalactic astronomy and cosmology: an introduction*. Springer, 2006.